Journal of Magnetic Resonance **137,** 46–58 (1999)
Article ID jmre.1998.1668, available online at http://www.idealibrary.com on IDEAL®

Principles and Performance of an Electron Spin Echo Spectrometer Using Far Infrared Lasers as Excitation Sources

H. P. Moll, C. Kutter,[1] J. van Tol, H. Zuckerman,[2] and P. Wyder

Grenoble High Magnetic Field Laboratory, Max-Plank-Institut für Festkörperforschung, Centre National de la Recherche Scientifique, B.P. 166, F-38042 Grenoble Cedex 9, France

Received February 19, 1998; revised November 18, 1998

We have built an electron spin echo spectrometer operating at 604 GHz, extending the frequency limit of existing spectrometers by more than a factor of 4. In order to handle this high frequency we have used optical techniques, i.e., molecular gas lasers for the excitation pulses and far infrared techniques for the heterodyne detection system. The different components of the spectrometer are described in detail and first experimental results are given.

1. INTRODUCTION

With the introduction of coherent pulsed techniques in nuclear magnetic resonance (NMR) and soon afterward in electron paramagnetic resonance (EPR), a new field opened for the investigation of the dynamics of spin systems. The formation of an echo after two excitation pulses, discovered and explained by E. L. Hahn, not only is fascinating but also allows the "memory" of a spin system to be studied by observing the echo intensity as a function of the time interval between the pulses. In their first experiments Hahn and his co-workers used sequences of two and three pulses to measure the spin-memory and spin–lattice relaxation times of nuclear spins (*1, 2*). The first electron spin echoes were observed with a modified NMR spectrometer working at 17.4 MHz and a static magnetic field of 6.2 G (*3*). Mims *et al.* (*4*) and Gordon *et al.* (*5*) used klystrons to create the excitation pulses working at 6.7 GHz. Kaplan *et al.* (*6*) constructed an X band (9 GHz) spectrometer based on pulsed magnetrons. With the strongly growing interest in pulsed ESR and the developments in microwave technology, the instrumentation improved enormously. The use of low power continuous wave (cw) sources in conjunction with a microwave switch and a traveling wavetube amplifier makes it possible to produce sophisticated multipulse sequences. Today, electron spin echo (ESE) spectroscopy is a very mature tool, comprising many different techniques such as electron spin echo envelope modulation, pulsed electron nuclear double resonance (*7*), and multidimensional techniques (*8*). Applications of the ESE technique have been reviewed in a number of articles (*9–11*).

Another development in recent years, in the fields of both NMR and EPR, has been to increase the operation frequency of the spectrometers in order to increase resolution and sensitivity. The resonance frequency of proton NMR is 850 MHz at 20 T, and intense pulses can be produced without many difficulties. In fact the upper frequency limit for high-resolution NMR is given by the availability of intense and homogeneous magnetic fields. The situation is somewhat different for EPR. Since the magnetic moment of the electron is three orders of magnitude larger than the magnetic moment of the proton, a magnetic field of 20 T corresponds to a resonance frequency of 560 GHz (for a g factor of 2). The upper frequency limit for ESE spectrometers is currently 140 GHz (5 T) (*12, 13*). The main constraint that limits a further increase of the frequency is the lack of suitably powerful microwave sources and equipment. High-field EPR was pioneered a long time ago by Lebedev (*14*). For cw EPR a 250-GHz spectrometer has been constructed (*15*) using a Gunn diode and a series of lenses for beam transport. A multifrequency spectrometer (0.25–1 THz) has been constructed by Brunel *et al.* (*16*) using a cw far infrared (FIR) laser as frequency source and using optical techniques. We have chosen a similar approach for doing pulsed EPR at high frequencies using pulsed FIR lasers.

There are several reasons to increase the frequency of the spectrometers. One of the most important is the increase in absolute sensitivity, which becomes obvious when we look at the radiated echo power being proportional to $\omega^4 N^2$, considering the rotating magnetization to radiate like a Hertz dipole. This would mean that, for an increase in frequency (ω) by a factor of 10, a hundred times fewer spins N can be detected, assuming that all the other components in the setup have the same performance. This, however, is far from the case for our experimental spectrometer. To mention only one problem, the transport of the radiation has high losses at high frequencies. It is clear from our studies that it will be very hard to increase the sensitivity of the existing spectrometers using far infrared techniques. However, there are a number of equally interesting

[1] Siemens Microelectronics Center, Königsbrücker Strasse, 180, 01099 Dresden, Germany.

[2] Life and Exact Sciences Department, The Open University of Israel, P.O.B. 39328, Tel-Aviv 61392, Israel.

1090-7807/99 $30.00

TABLE 1
Comparison of the Elements of Various Pulsed EPR Spectrometers: 9.5, 95 (Leiden Spectrometer), 140 (MIT Boston), and 604 GHz (Grenoble)

	9.5 GHz 0.34 T	95 GHz 3.4 GHz	140 GHz 5.0 T	604 GHz 21.5 T
Source	Gunn diode TWT amplifier	IMPATT diode IMPLO	Gyrotron	FIR laser
Power	~kW	210 mW	~200 W	~100 W
Pulse width	8 ns	30 ns		100 ns
Switch	PIN diode	PIN diode	PIN diode	Plasma switch (not used)
Radiation transport	Fundamental waveguides	Fundamental and oversized waveguides	Fundamental and oversized waveguides	Fundamental and oversized waveguides
Cavity	Cylindrical	Cylindrical	Fabry–Perot	Fabry–Perot-type
Detector	Mixer phase-sensitive	Mixer phase-sensitive	Mixer phase-sensitive	Schottky diode not phase-sensitive
Static B field	Resistive Helmholz coils	Superconducting coil	Superconducting coil	Resistive coil

points or advantages appearing at high frequencies/high magnetic fields: (1) The Zeeman splitting at 604 GHz corresponds to 29 K, so that at liquid helium temperatures, the spin polarization of the levels is almost complete (99.8% at 4.2 K), while at room temperature, we still have a 5% polarization. This high polarization presents an interesting physical situation, which may lead to very long spin-memory times (*17*). (2) The high frequencies create the possibility of studying the energy (or magnetic field) dependence of the spin–lattice (T_1) and spin–spin (T_2) relaxation times over a much wider range. New insight into the relaxation processes can be expected by performing studies of T_1 and T_2 as functions of the magnetic field (*18*). (3) The 60-fold increase in frequency with respect to X band facilitates measurement of small g anisotropies and simplifies interpretation of the spectra. For powders with badly resolved g anisotropy at low field, the high-frequency spectrum may reflect the orientation dependence of g and creates the possibility of selecting an orientation by selecting a field position within the EPR spectrum. (4) High-spin systems ($S \geq 1$) with much larger zero field splittings can be studied, since the photon energy of the high field spectrometers is much higher (*19*, *20*).

2. CONCEPTS AND SETUP OF THE SPECTROMETER

In an electron spin echo experiment one needs on the one hand relatively intense pulses and on the other the possibility of detecting the low-intensity response (the echo). Conventional spectrometers work at X band frequencies (9.5 GHz) and magnetic fields around 0.3 T (*21*, *22*). The problem of constructing a high-frequency ESE spectrometer is that microwave elements used at low frequencies cannot be used at frequencies higher than 500 GHz or are simply not available.

In Table 1 we present a comparison between the spectrometer elements that are used at 9.5, 95, and 140 GHz and the elements we used at 604 GHz.

For an electron-spin-echo experiment, short pulses with high power are required in order to excite the spin system. At 9 GHz, power levels on the order of kW are achievable and allow use of very short pulses of around 8 ns. The Leiden spectrometer (*12*) has a power level of only 210 mW, but, together with a high Q cylindrical cavity, it can use pulses with a length of around 30 ns. Powerful sources around 600 GHz are gyrotrons, free electron lasers, or pulsed far infrared lasers. The free electron laser is a rather large installation, and a 600-GHz gyrotron is not standard equipment which can be bought. Therefore, these sources have not been considered for this work. The only practical sources in this frequency range are, at the moment, pulsed FIR lasers. Another advantage of pulsed FIR lasers is that they have an intrinsic pulse width of about 100 ns, and no switch is needed for the generation of the high-frequency pulses.

A frequency of 600 GHz corresponds to a wavelength of 0.5 mm, and, as a result, the transport of the radiation in fundamental-mode waveguides, as used in low-frequency EPR, would cause unacceptable losses. A purely optical solution with lenses and mirrors (*23*) would require many optical elements and its alignment would be very critical. We have opted for a solution halfway between microwave and optical techniques, namely oversized waveguides with a diameter 20 times the wavelength.

At low frequencies, fundamental-mode cavities such as rectangular or cylindrical cavities are used with cavity dimensions or the order of the wavelength. Since the design of a fundamental-mode cavity at 0.5 mm seems to be very difficult, we selected a quasi-optical Fabry–Perot-type cavity with a low finesse of about 40.

The requirements for the detector are good time resolution (on the order of nanoseconds) and high sensitivity. Here, we can profit from the enormous progress which has been made in the field of radio astronomy, where very sensitive heterodyne detectors have been developed for spectroscopic applications (*24*). These detectors, using a Schottky diode as mixer, offer both a high sensitivity and a very good time resolution.

The last point in Table 1 is the static magnetic field. A frequency of 604 GHz corresponds to a magnetic field at resonance of 21.5 T, which can at present be generated only

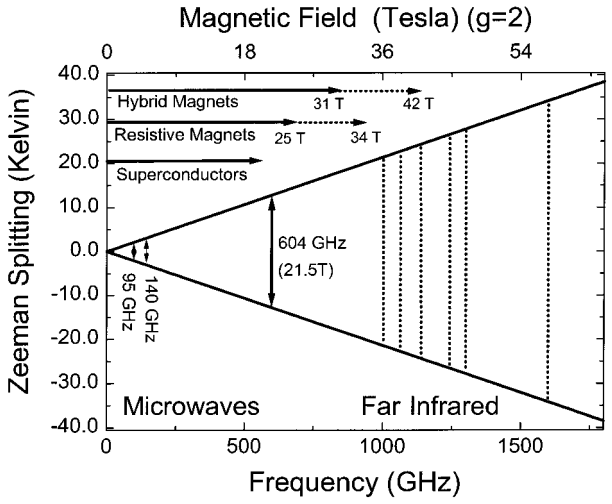

FIG. 1. Zeeman splitting for spin $\frac{1}{2}$ and g factor 2 as a function of the magnetic field (top axis). On the bottom axis the corresponding frequency for an ESE spectrometer is shown. Spectrometers up to 140 GHz have been realized using microwave techniques. Several strong laser lines, suitable for ESE spectrometers, are indicated as dotted lines. We show the magnetic field limits for the Grenoble polyhelix and hybrid magnet.

by resistive magnets (see Fig. 1). The magnet used for our experiments is a polyhelix magnet (*25*) with a power supply of 10 MW.

Figure 2 schematically shows the experimental setup of the 604-GHz spin echo machine. The main elements will be described in more detail in the following sections, but here we will give a brief overview.

A master pulse generator triggers the two FIR laser systems and the electronic switch in the detection system. In this way two independent FIR excitation pulses with every possible delay can be generated. The laser pulses are spatially overlaid and are directed into the cavity, which is positioned in a variable-temperature flow cryostat (4.5–300 K). In order to keep the losses minimal the FIR lasers have been placed close to the magnet, the bore of which is positioned horizontally. All the optical elements have been situated in this horizontal plane to make the alignment as simple as possible. The reflection cavity can be adjusted from the back side of the magnet during the experiment. The returning echo is reflected by a beam splitter in the direction of the Schottky diode, which is operated as a heterodyne detector. The 7-GHz difference frequency of the signal and a local oscillator (a cw FIR laser at 611 GHz) is electronically amplified, rectified, and recorded with a fast transient digitizer.

3. COMPONENTS

A. Generation of FIR Pulses

One of the main technical obstacles in the construction of a high-frequency electron spin echo spectrometer is the generation of short π and $\pi/2$ pulses. The required magnetic field of the FIR radiation for a π pulse is given by the relation

$$\pi = \gamma \Delta t B_1, \qquad [1]$$

γ being the gyromagnetic ratio, Δt the pulse width, and B_1 the amplitude of the magnetic field of the FIR radiation. The relation between the magnetic field and the power density (P/A) of a free propagating wave is given by the Poynting relation

$$\frac{P}{A} = \frac{c(2B_1)^2}{2\mu_0}, \qquad [2]$$

A being the sample area and μ_0 the permeability of free space. For an assumed Δt of 100 ns a magnetic field B_1 of 1.8 G at the sample position (10 mm^2) is needed, corresponding to a required power of 75 W. The factor of 2 for the magnetic field amplitude ($2B_1$) in Eq. [2] enters because the applied FIR light is linearly polarized, while only one circularly polarized component (B_1) is effective on the spins. One can see that pulses shorter than 100 ns need very high power levels (see Table 2). Lasers providing these high power levels can be Raman FIR lasers pumped by multiatmospheric-pressure transversally excited CO_2 lasers. Power levels of MW/cm^2 are reported for pulse durations on the order of nanoseconds (*26*).

For very long pulses with, for example, 1 μs pulse width, even cw FIR lasers can be considered to be high-frequency sources. Typical power levels of continuous wave FIR systems

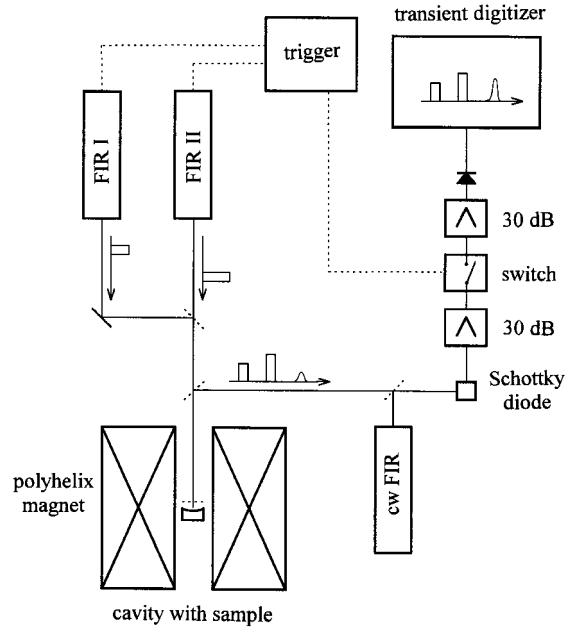

FIG. 2. The schematic setup of the 604-GHz spectrometer. Three main elements can be distinguished: (1) The pulsed FIR lasers with the light pipes and the cavity, (2) the heterodyne detector, and (3) the static magnetic field B_0.

TABLE 2

Comparison between the Pulse Width and the Required FIR Power (Assumed Sample Area 10 mm^2; Without Use of a Cavity)

	Δt			
	1 μs	100 ns	10 ns	1 ns
P	750 mW	75 W	7.5 kW	0.75 MW
Source	cw FIR	TEA–laser pumped FIR laser	Raman FIR laser	

TABLE 3

Pulsed FIR Laser Lines with a Close by Local Oscillator Line

Frequency (GHz)	FIR gas	Pump line	Local oscillator	$\Delta\nu$ (GHz)
246.31	MF13	9P (32)	MI 239.3 GHz 10P (32)	7.0
604.30	MF	9P (20)	DMI 611.3 GHz 9R (22)	7.0
989.4	MF	9R (18)	FAC 985.9 GHz 10R (24)	3.5
1145.1	MF	9R (24)	CDF 1153 GHz 10R (20)	7.9
1244.0	MF	9R (28)	CDF 1236 GHz 10R (14)	8.0
1295.8	MF	9R (30)	CDF 1298 GHz 10R (38)	2.2
1550.9	MF	9R (40)	MF 1555 GHz 10R (32)	4.1

Note. $\Delta\nu$ is the intermediate frequency between excitation pulse and local oscillator. The following gases are used: MF, methyl fluoride; MF13, methyl fluoride with ^{13}C isotope; MI, methyliodide; DMI, fully deuterated methyliodide; FAC, dideuteroformic acid; and CDF, cis-1,2-difluoroethylene.

are on the order of 1–100 mW and could be obtained from convenient high-frequency sources together with a high-quality cavity. In such a system the cw–CO_2 laser could be switched with the help of a Pockels cell switch consisting of a polarizer, a CdTe crystal, which rotates the polarization proportional to the applied electric field (Pockels effect), and an analyzer. The switching times of Pockel cells are very fast (in the nanosecond range); however, the buildup of the radiation in the FIR cavity is not instantaneous. Pulses with a width of about 1 μs can be generated with this technique (*27*).

The typical line shape of the TEA–CO_2 laser pulse is characterized by an intense peak ($\approx$200 ns) followed by a long tail ($\approx$1 μm) due to the energy storage of the admixed N_2 molecule to the laser gas. In Fig. 3 we show that the response from the FIR laser is quasi-instantaneous and for low pressures of the FIR gas the shape of the FIR pulse is comparable to the shape of the pump pulse. Since for the ESE experiment a single FIR pulse is required, lasing of the tail has to be suppressed. This can be achieved by increasing the FIR gas pressure slightly and thus increasing the FIR lasing threshold.

The output power of the laser lines of our FIR laser systems listed in Table 3 is depicted in Fig. 4. Since the maximum field of the magnet chosen for the experiments is around 25 T, the frequency of the excitation pulses should not be higher than 700 GHz if we assume a spin system with $g = 2$. In this case only two laser lines, the one at 246 GHz (8.786 T) and the one at 604 GHz (21.571 T), are in our magnetic field range. Figure 4 shows clearly that the power levels we obtained from these lines are still below the required powers. However, the condition of the $\pi/2$ and π pulses can still be met by means of a cavity. In this way the effective power at the sample position is amplified by several orders of magnitude (see Section C).

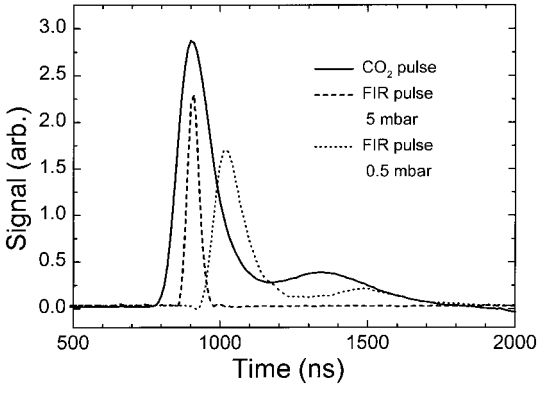

FIG. 3. Pulse shapes for pump laser (TEA–CO_2 laser, 9P20) (solid line) and far infrared laser with methyl fluoride at low pressures (dotted line) and high pressures (dashed line).

B. Two- and Three-Pulse Configurations

Three different configurations have been used to produce the two/three pulse sequences (see Fig. 5). Two FIR pulses can be generated with the help of an optical delay line, where the CO_2 pulse is split into two parts. One part is directly fed into the FIR cavity; the other part is optically delayed and then focused into the FIR cavity. Using a path difference of 90 m, a time delay of 300 ns has been achieved between the two pulses. The

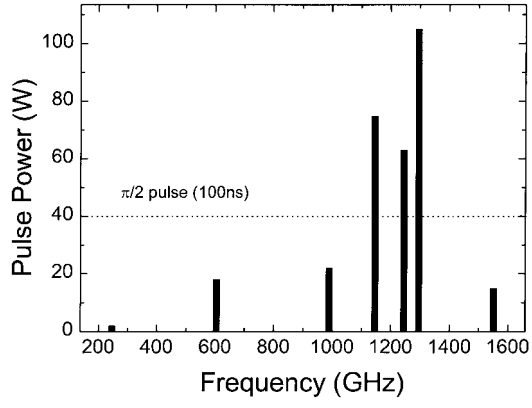

FIG. 4. Typical power levels of our pulsed FIR laser system for different pump lines of the CO_2 laser (see Table 3). The dotted line is the power required for $\pi/2$ pulses assuming a pulse length of 100 ns. In this estimate no cavity is taken into account. When a cavity is used the effective power at the sample position can be increased and lower FIR power levels are required.

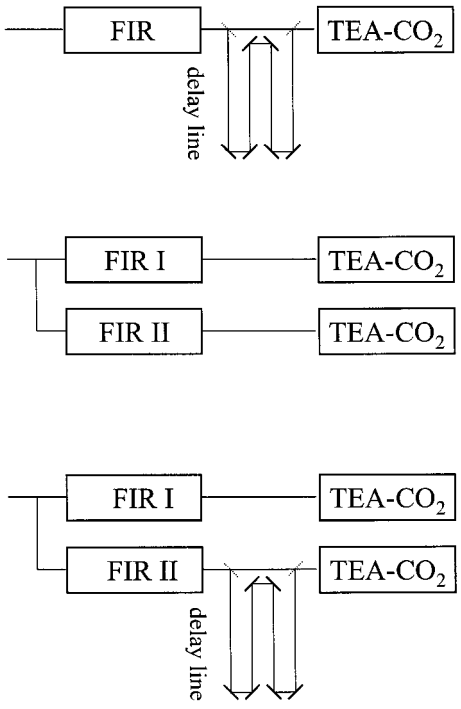

FIG. 5. (a) Two-pulse sequence using an optical delay line. (b) Two-pulse sequence using two independent FIR laser systems. (c) Three-pulse sequence combining (a) and (b).

delayed CO_2 laser beam has been focused several times on its path with long focal length concave mirrors and has only been attenuated about 50%. The advantage of this setup is that both pulses are generated in one cavity, and no problems such as different frequencies of the two excitation pulses or time jitters occur. This configuration has been shown to be the simplest excitation sequence. However, it has the disadvantage that the delay between the two pulses cannot be varied during an experiment.

For a two-pulse sequence, where the delay between the two pulses can be varied, two independent CO_2 lasers and two independent FIR lasers are required. Special care has to be taken that both FIR lasers emit the same frequency, which has been achieved by tuning the FIR laser cavity length. Since we had no equipment to determine a frequency shift between both lasers, we optimized the FIR cavities on the echo signal.

In this configuration the TEA–CO_2 lasers are triggered electronically and each shows a time jitter on the order of 20–50 ns between the trigger pulse and the optical output. This adds up to a total jitter of 70 ns between the two FIR pulses.

The three-pulse sequence consists of a combination of both of the above-described configurations and is very appealing because the whole setup can be optimized on the echo sequence of the FIR laser with the optical delay line. After this step all the parameters are kept fixed, and only the second laser has to be optimized on the echo signal.

All three configurations have been tried out and used in this work and have proven to be suitable excitation sequences for the spin-echo experiment.

C. Radiation Transport and Cavity

For most of the standard FIR experiments the only interesting parameter for the radiation transport is the transmitted power, and hollow metallic light pipes (polished brass tubes) have proven very suitable. A beam which initially has a well-defined polarization and spatial Gaussian properties loses them after being transported in these light pipes over a relatively short distance (≈10 cm–1 m) (*28*).

In our experiment we are interested in coupling a TEM_{00} mode into the Fabry–Perot cavity in order to have well-defined cavity behavior (deep and sharp dips in the reflected power as a function of the mirror distance; see next section). The TEM_{00} can be launched when the incoming beam has well-defined polarization and spatial Gaussian properties. The task in the beam transport is, therefore, to conserve these two properties.

We recall the transmission characteristics of oversized waveguides. The field distribution in a metallic waveguide is given by the TE_{mn} and the TM_{mn} modes, which are the solutions of the Maxwell equations for special boundary conditions. The attenuation $\alpha(\lambda_0)$ for the TE_{mn} mode in a circular waveguide with diameter $2a$ is given by (*24, 29, 30*)

$$\alpha(\lambda_0) = \frac{0.023 R_s}{\sqrt{1-\left(\frac{\lambda_0}{\lambda_c}\right)^2}}\left[\frac{m^2}{\chi'^2_{mn}-m^2}+\left(\frac{\lambda_0}{\lambda_c}\right)^2\right] \quad \left[\frac{\mathrm{dB}}{\mathrm{m}}\right] \tag{3}$$

where χ'_{mn} is the nth nonvanishing root of the derivative of the mth-order Bessel function. For copper R_s is $0.00825\sqrt{f}\,\Omega$ (frequency f in GHz). The free-space wavelength (λ_0) of our pulsed laser is 0.496 mm. The cutoff wavelength (λ_c) for the TE_{mn} mode is given as

$$\lambda_c = 2\pi a/\chi'_{mn}. \tag{4}$$

If we use the TE_{11} mode in a 0.4-mm-diameter waveguide so that only this mode is allowed (fundamental waveguide), we obtain an attenuation of 42 dB/m, a value for which the waveguide should be called an absorber rather than a waveguide. When we choose a waveguide diameter of 1.0 mm we obtain an attenuation of 9.0 dB/m and if we take a diameter of 10 mm we obtain an attenuation of 0.76 dB/m—a reasonable value.

The TE_{11} mode is a mode with a defined polarization. However, in the circular metallic waveguide, the lowest loss modes are modes (TE_{0n}) with a radial electric field distribution where a polarization cannot be defined. If no care is taken when using the circular oversized waveguides, a number of

modes are launched. Due to their low loss the TE_{0n} modes are dominant after a short distance, and the FIR radiation has lost its polarization.

For this reason it is interesting to work with dielectric quartz tubes where the lowest loss mode is the hybrid EH_{11} mode, a mode with well-defined polarization. The attenuation for the EH_{11} mode in oversized waveguides is given by

$$\alpha(EH_{11}) = 1.826 \frac{\lambda_0^2}{a^3} \left[\frac{dB}{m}\right]. \quad [5]$$

For a 10-mm-diameter waveguide we obtain a value of $\alpha = 3.65$ dB/m, corresponding to an attenuation of 57% per meter.

In the experimental praxis a number of modes are simultaneously launched and a prediction of the transmitted power depends strongly on which waveguide modes are excited. Furthermore, a discontinuity in the waveguide (e.g., windows and corner pieces) may lead to conversion of one mode into another waveguide mode. For the spin-echo experiment it has been important to minimize the attenuation while conserving the polarization and Gaussian properties of the beam. Therefore, we tried to use the TE_{11} metallic and the EH_{11} dielectric waveguide modes, which couple well to the free-space Gaussian beam (TEM_{00}). We successfully tried the dielectric oversized waveguides and the circular metallic waveguides. However, for both types of waveguides we saw that the cavity behavior depends critically on the alignment of the waveguide axis on the optical axis of the experiment. For slightly misaligned waveguides, bad or no cavity structure may be observed.

The magnetic field B_1 of the FIR pulses at the sample position can be enhanced by the use of a cavity. In these terms the cavity is used as an amplifier of the FIR radiation. Another method for increasing the B_1 field at the sample position would be to focus the radiation with the help of a lens. The use of a cavity, however, has additional advantages: When the setup is used as a cw spectrometer, the sensitivity is drastically increased by the cavity. Another advantage is that, when tuned to resonance, the reflected power of the FIR pulses is minimal and the lifetime of the Schottky diode is increased.

Due to the short wavelength we have not opted for a microwave-type cavity (i.e., a cylindrical, rectangular cavity), but have chosen a Fabry–Perot-type reflection cavity, consisting of one semitransparent mirror and one reflecting concave mirror.

In order to calculate the enhancement of the intensity in the cavity, we write the circulating field B_1^{cavity} in the cavity as a sum of the individual components of the multiple reflected beams in the cavity, illustrated in Fig. 6 (*31, 32*). When the cavity is tuned to resonance, the distance of the mirrors d is a multiple of half of the wavelength, the phase factor ($e^{i\delta}$ with $\delta = 4\pi d/\lambda$) of the individual components becomes unity, and we can write for the maximum of the magnetic field

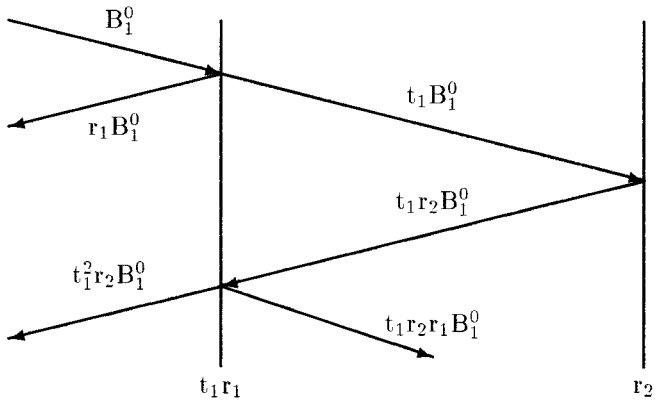

FIG. 6. Principle of the Fabry–Perot-type cavity.

$$B_1^{\text{cavity}} = t_1 B_1^0 (1 + r_2 + r_1 r_2 + r_1 r_2^2 + r_1^2 r_2^2 + \cdots) \quad [6]$$

$$= B_1^0 \frac{t_1(1 + r_2)}{1 - r_1 r_2}, \quad [7]$$

where t_1^2 is the transmission coefficient of the first mirror and r_1^2 is its reflection coefficient. Since the second mirror is not ideal we assume a reflectivity of r_2^2. For simplicity we include all the other losses (absorption mesh and mirror, diffraction losses) in the cavity in this factor r_2^2. For the intensity we obtain

$$\frac{I^{\text{cavity}}}{I^0} = \frac{t_1^2(1 + r_2)^2}{(1 - r_1 r_2)^2}. \quad [8]$$

For the cavity used we have $t_1^2 = 0.1$, $r_1^2 = 0.9$, and $r_2 = 0.98$, and we obtain an enhancement in intensity of about 20 and an enhancement of the magnetic field B_1 by a factor of 4.5.

To calculate the back-reflected intensity of the cavity we have to consider the interference of all the parts of the beam which leave the cavity in the incoming direction:

$$B^{\text{ref}} = B_0 r_1 e^{-i\omega t} - [B_0 t_1^2 r_2 e^{-i(\omega t + \delta)} + B_0 t_1^2 r_2^2 r_1 e^{-i(\omega t + 2\delta)} + B_0 t_1^2 r_2^3 r_1^2 e^{-i(\omega t + 3\delta)} + \cdots]. \quad [9]$$

Evaluating Eq. [9] and forming $B^{\text{ref}} B^{\text{ref}*}$, we come to the well-known Airy formulas for the reflected intensity

$$I_r = I_0 \frac{(r_2 - r_1)^2 + 4 r_1 r_2 \sin^2(\delta/2)}{(1 - r_1 r_2)^2 + 4 r_1 r_2 \sin^2(\delta/2)}. \quad [10]$$

In Fig. 7 the reflected power is shown as a function of the mirror distance with the reflectivity of the first mirror as parameter. One can see that the back-reflected power is minimal when r_1 is equal to r_2. This situation is called critical coupling of the cavity and is important for the best sensitivity when cw EPR is performed.

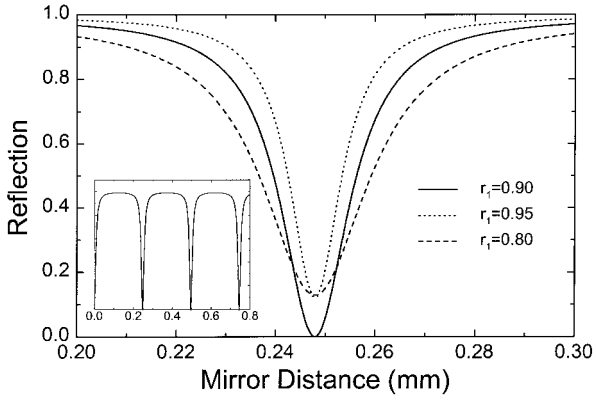

FIG. 7. Reflected power in a Fabry–Perot-type reflection cavity as a function of the mirror distance. The parameter r_1 is the reflectivity of the first mirror ($r_2 = 0.9$). The inset shows a wider range for the scanned mirror distance.

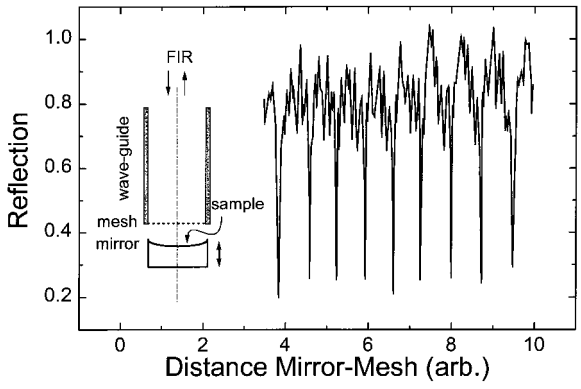

FIG. 8. The cavity used has a curved back mirror and a mesh as first mirror. Scanning the rear mirror the cavity resonances can be recorded. We obtain a finesse of about 40.

Another interesting number of a cavity is its finesse, which is defined as (*31*)

$$F = \frac{\pi\sqrt{r_1 r_2}}{1 - r_1 r_2} \approx \frac{\delta\lambda_{ax}}{\delta\lambda_{\text{cav}}}, \qquad [11]$$

where $\delta\lambda_{ax}$ is the spacing between two resonances, and $\delta\lambda_{\text{cav}}$ is the FWHM of one resonance peak. We should remark that, for a Fabry–Perot-type cavity, the figure of merit is its finesse and not its Q value, because Q depends on the number of half wavelengths the cavity is tuned to. For the first resonance $Q = F$ and for the nth resonance $Q = nF$, so Q can obtain a very high (for our purpose meaningless) number (*33*).

The ringing time of the cavity, the time in which a stationary cavity intensity I^{cavity} decays to $1/e$ of its value after the incoming intensity is suddenly switched off, is given as

$$\tau_c \approx \frac{1}{2\pi\delta\nu} = \frac{Q}{\omega}. \qquad [12]$$

In our case Q ($=nF$) is about 200 ($=4 \times 50$ for the fourth resonance), and ω is 2π 604 GHz, resulting in a ringing time of about $\tau_c \approx 5.3\ 10^{-11}$ s. Due to the high frequencies, cavities with much higher Q than used at microwave frequencies can be taken. In the above considerations of the plane parallel cavity we did not consider the losses of the radiation which escapes to the side (diffraction losses). Especially at long wavelengths, when the beam has a large divergence, the intensity is strongly reduced after a few cavity round trips. We can minimize this effect by choosing a semiconfocal configuration, where one of the mirrors is curved. The cavity used is shown in Fig. 8 and consists of a mesh and a curved rear mirror, with a radius of curvature which is matched to the wavefront of an assumed Gaussian beam (TEM_{00}) which leaves the waveguide.

The 200 lines/inch mesh (*32*) has been selected by trial and error optimizing the depth of the resonances and the finesse of the cavity. The measured finesse ($\delta\lambda_{ax}/\delta\lambda_{\text{cav}}$) of the loaded cavity is about 40 and corresponds approximately to the theoretical considerations mentioned before.

In this cavity the magnetic field of the standing waves has maxima at the mirror surfaces and half wavelengths in between (see Fig. 9). In order to have the maximum magnetic field at the sample position the sample has been glued at the back mirror.

D. Schottky Diode Heterodyne Detector

The requirements of the detector are a high sensitivity (≈nW), a high time resolution (≈ns), and a high dynamic range (10^6). The high dynamic range is required because the strong excitation pulses, which precede the echo, should not saturate or destroy the Schottky diode. To protect the diode, one might use an optical switch, which can be opened when the echo is expected. At 604 GHz the only fast optical switch that is currently known consists of a semiconductor slice (e.g., Si) which is transparent for FIR radiation and can be made reflec-

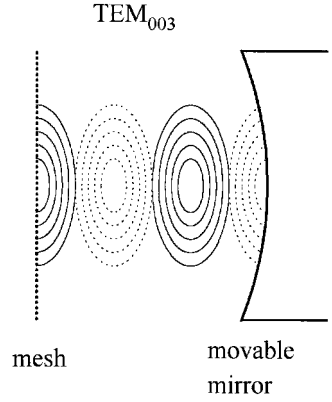

FIG. 9. Contour plot of the magnetic field for the TEM_{003} mode in the Fabry–Perot cavity. The dotted lines are for negative contour levels. The magnetic field has local maxima with a spacing of $\lambda/2$. Note that there are local maxima on the surface of the mesh and the curved mirror.

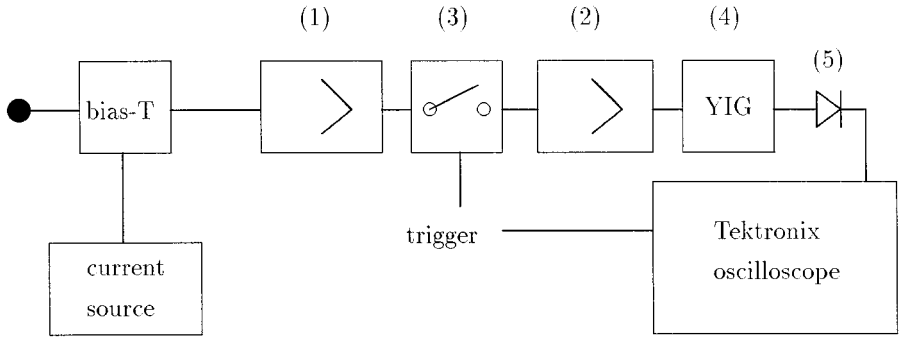

FIG. 10. Electronic components of the heterodyne receiver. The numbers correspond to the elements of Table 4.

tive by the creation of a very dense carrier plasma, for example, by illumination with a strong Nd–YAG laser pulse (*34*). In a single stage such a switch can provide an isolation of 20 dB with a loss as small as 10%. Since such a switch requires an additional synchronized laser, it has not been used in the present setup. In our case the Schottky diode withstands the high power levels of the excitation pulses, so no direct protection is used. However, the amplifiers following the rectified signal show saturation effects. This problem has been solved by introducing a fast HF switch after the first amplifier (see Fig. 10 and Table 4).

When the Schottky diode is used as a radiation detector, the operation principle can be seen in the following way: The electric field of the light over the contact modulates the applied bias voltage. In video detection (*35*) this leads to an additional current ΔI. By biasing the Schottky diode with a current source, this ΔI is transformed into a ΔV_{signal}. For small light intensities P, the diode behaves like a quadratic detector ($V_{\text{signal}} \approx P$), and for large intensities, like a linear detector ($V_{\text{signal}} \approx \sqrt{P}$).

The effect of mixing two frequencies (ω_1, ω_2), which are sent simultaneously, on the Schottky diode can be seen by a simple Taylor expansion of the current $I(V(t))$ around the bias point V_0 (*35*):

$$I(V(t)) = I(V_0) + \left(\frac{\partial I}{\partial V}\right)_{V_0} V + \left(\frac{1}{2}\frac{\partial^2 I}{\partial V}\right)_{V_0} V^2 + \cdots . \quad [13]$$

Taking $V(t) = V_0 + V_1\sin(\omega_1 t) + V_2\sin(\omega_2 t)$ and neglecting terms higher than second order leads to

$$\begin{aligned} I(V(t)) = I(V_0) &+ \left(\frac{\partial I}{\partial V}\right)_{V_0}(V_1\sin(\omega_1 t) + V_2\sin(\omega_2 t)) \\ &+ \frac{1}{2}\left(\frac{\partial^2 I}{\partial V^2}\right)_{V_0}[V_1^2 + V_2^2 + V_1^2\cos(2\omega_1 t) \\ &- V_2^2\cos(2\omega_2 t) + V_1V_2\cos((\omega_1 - \omega_2)t) \\ &+ V_1V_2\cos((\omega_1 + \omega_2)t)] + \cdots , \end{aligned} \quad [14]$$

where the sum $(\omega_1 + \omega_2)$ and difference $(\omega_1 - \omega_2)$ frequencies occur. It can be seen that the term with the difference frequency is proportional to V_1V_2. Even for a very weak signal amplitude (V_1), we can obtain a strong mixing term when the local oscillator amplitude (V_2) is high. However, the important number of a heterodyne receiver is not the absolute value of the mixing term, but the signal-to-noise ratio or the system noise temperature.

Since the best system noise temperatures for Schottky diodes are obtained for local oscillator powers on the order of mW, cw FIR lasers are used (611-GHz line of fully deuterated methyl-iodide CD_3I; CO_2 pump line: 9R22).

The system noise temperature is defined as the temperature an ohmic resistor would have when producing the same noise power at its output as the noise power of the system. It consists of the noise temperature of the mixer (T_{mix}) and the noise temperature of the first, low-noise amplifier (T_{IF}) times the conversion loss (L):

$$T_{\text{sys}} = T_{\text{mix}} + LT_{\text{IF}}. \quad [15]$$

TABLE 4
Microwave Elements Used in the Heterodyne Detection System

		Gain	Bandwidth (GHz)	Noise figure (dB)
(1)	MITEQ AFS4-04000800-08-10P4	30 dB	4–8	0.8
(2)	MITEQ AFS4-01000800-25-10P4	30 dB	1–8	2.5
(3)	Switch Innovat. Microw. Tech.		1–18	
(4)	YIG filter (Computer Solutions)		1–18 ΔB: 30 MHz	
(5)	Schottky diode EMC Tech.		0–18	

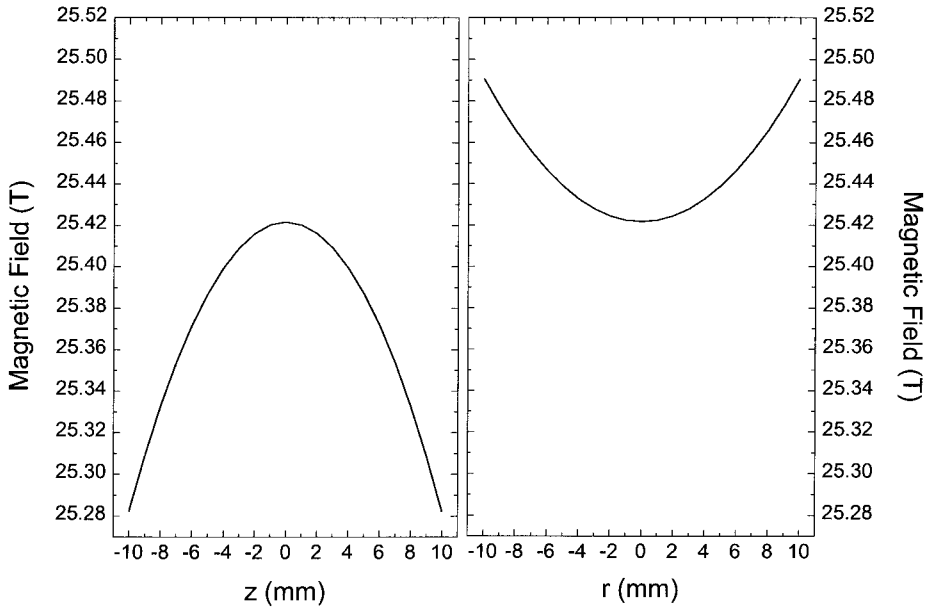

FIG. 11. Calculated field profile of the Grenoble polyhelix magnet.

The conversion loss is the ratio between incoming power at the detector and the power of the generated intermediate frequency. It is mainly influenced by the antenna characteristic of the mixer block and the quality of the contact. Typical values for the conversion loss are of the order of 10–50. The mixer has typical values of $T_{\text{mix}} = 2000$ K. It is obvious that a low T_{IF} is important in order to reach the best system noise temperatures. Therefore, the intermediate amplifier is normally cooled (for simplification we did not cool the IF amplifier in our experiment).

The standard technique in radioastronomy for determining the system noise temperature is to perform a cold–hot measurement, where the signal is given by a blackbody radiator at 77 K and at room temperature (*36*).

Experimentally, we can obtain three values,

$$V_{\text{hot}} = \alpha(T_{\text{hot}} - T_{\text{sys}}), \quad [16]$$

$$V_{\text{cold}} = \alpha(T_{\text{cold}} - T_{\text{sys}}), \quad [17]$$

the voltage when the hot (cold) load is connected (with a constant α), and

$$\Delta V = V_{\text{hot}} - V_{\text{cold}}, \quad [18]$$

the signal on the lock-in amplifier when the cold source is chopped. The system noise temperature is then given as

$$T_{\text{sys}}^{\text{DSB}} = \frac{V_{\text{hot}} + V_{\text{cold}}}{2}\frac{\Delta T}{\Delta V}, \quad [19]$$

where DSB (double sideband) signifies that both the lower and the upper sideband with respect to the LO frequency have been measured ($\nu_{\text{LO}} - \nu_{\text{IF}}$ and $\nu_{\text{LO}} + \nu_{\text{IF}}$).

For the present setup we determined a system noise temperature of 60,000 K, corresponding to a noise equivalent power (NEP $= k_B T_{\text{sys}}$) of 8×10^{-19} W/Hz. Since the best reported values for these kind of diodes are 2000 K, a factor of 30 can still be gained in sensitivity (*24*).

E. Homogeneity of the Polyhelix Magnet M9

The magnet used for the spin-echo experiment is the polyhelix magnet M9 at the Grenoble high-magnetic-field laboratory. It is a 10-MW magnet which uses a combination of eight inner helical coils, an inner Bitter stack, and an outer Bitter stack, delivering a magnetic field of up to 25 T (*25*). Since this magnet has been optimized only on the maximum magnetic field, it has a relatively poor spatial homogeneity (see Fig. 11).

The temporal stability of resistive magnets is mainly given by the current fluctuation of the power supplies. For us only low-frequency variations are important because a copper cylinder around the sample chamber shields noise above 10 kHz very well. The remaining fluctuations are in the frequency range below 1 kHz, with an amplitude of about 10 G p–p at maximum field.

The spatial and temporal magnetic field inhomogeneities currently limit EPR applications of resistive magnets to samples with linewidths larger than 10 G.

F. Fluctuations and Time Jitters

There are a number of elements involved in the experimental setup that contribute to a fluctuation of the echo amplitude.

TABLE 5
Specifications of the 604-GHz Spectrometer

Frequency/B field	604 GHz/21.5 T
Pulsewidth	100 ns
No. of pulses	2 or 3
Sensitivity	3×10^{12} spins per G
Temperature range	4 K up to 300 K
Sample restrictions	linewidth >10 G

They have already been discussed in the previous sections and are summarized here.

The excitation pulses have a fluctuation both in amplitude and in time. In a well-maintained laser system the amplitude fluctuation can be reduced to about 10%. More serious is the time jitter of the delay between the two pulses, which amounts to about 70 ns. For very long T_M times it does not disturb the measurements; however, it leads to an enormous jitter of the echo amplitude for short relaxation times. This jitter depends only on the thyratron and the spark gap of the TEA–CO_2 lasers and can be minimized by proper maintenance of these elements. However, the time jitter is no principal restriction, because it can be eliminated by software, by recording the echo signal together with the actual delay between the excitation pulses and counting into channels.

The static magnetic field shows low-frequency fluctuations. Over one echo sequence the static magnetic field is constant; however, it varies between two consecutive pulse sequences with a mean amplitude of about 10 G p–p (at 22 T). The value of 10 G p–p is an estimate for "good" days and has been much higher for other measurement days (depending on the performance of the 20-MW power supply). This fluctuation leads to the fact that the echo signal is always due to another spin packet in the resonance line. It becomes the dominant fluctuation when samples with very small linewidths are studied. An extreme example is the measurement on BDPA with a linewidth of about 10 G. Here, the sample was literally in and out of resonance between two consecutive echo sequences.

The amplitude of the cw FIR laser shows fluctuations or drifts in the power. Although this problem is well known, and many solutions have been proposed (*37*) to stabilize the power, in practice it limits the measurement possibilities on many days.

4. RESULTS

To describe the capabilities and limitations of our 604-GHz ESE spectrometer (see Table 5 for specifications) we will briefly describe the results of measurements on the spin labels TEMPO (2,2,6,6-tetramethyl-1-piperidinyloxy) and BDPA (α,γ-bis diphenylene-β-phenylallyl 1:1 complex with benzene), which was dispersed in polystyrene and deposited as a film on the back mirror of the cavity. These free radicals have been chosen because it is easy to vary the concentration and the number of spins.

The first echoes we observed were generated with a single far infrared laser and an optical delay line to realize a two-pulse sequence with a fixed time delay of 300 ns. One of the first results is presented in Fig. 12. There the excitation pulses occur smaller than the echo which is due to an electronical switch placed in our amplification circuit to avoid saturation of the amplifiers caused by the intense excitation pulses. The switch opens after the pulses and enables us to detect the spin-echo signal (attenuation of the switch: 30 dB).

The electron spin echo can be used to detect an EPR spectrum by recording the height of the echo while sweeping the external magnetic field. In our experiment we used an oscilloscope (Tectronix TDS 644A) which has the option to set two cursors and integrate the enclosed signal. In this way the echo height has been recorded during the field sweep.

In a first experiment we measured the EPR spectrum of BDPA in polystyrene (1:10) at the frequency of 604 GHz and a temperature of 8 K (see Fig. 13). The sweep rate of the magnetic field was 1 G/s. The shape of the spectra can be reasonably well fit by a Gaussian curve with a full width at half maximum of 8.9 G. The strong fluctuation of the echo signal is due to irregularities of the excitation pulse power and the temporal instability of the magnetic field, which are in the order of about ± 5 G. Averaging over several echoes is limited because of the low repetition rate (8 Hz). However, one should be careful with the interpretation of the measured lineshape, because the linewidth is comparable to magnetic field fluctuations. For the measurement of narrow resonance lines one would have to install an active field stabilization to compensate the field fluctuations below 1 kHz. Higher frequencies can be easily filtered out in a passive way by using a copper shield.

The electron spin echo experiment offers the opportunity to determine the spin memory time T_M, which is often related to the spin–spin relaxation time T_2:

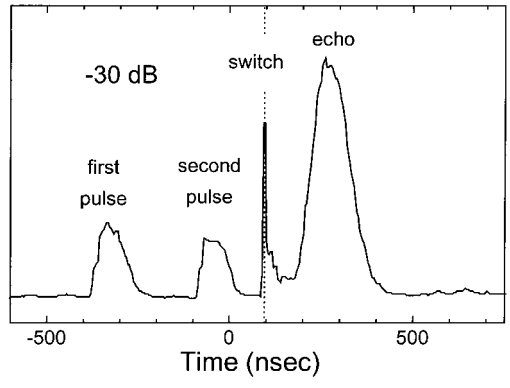

FIG. 12. Two-pulse spin echo sequence on BDPA in a polystyrene matrix. The frequency of the pulses is 604 GHz leading to a resonance position of 21.4415 T. The graph is a single shot taken at 8 K. The excitation pulses are attenuated by 30 dB with the help of an electronic switch.

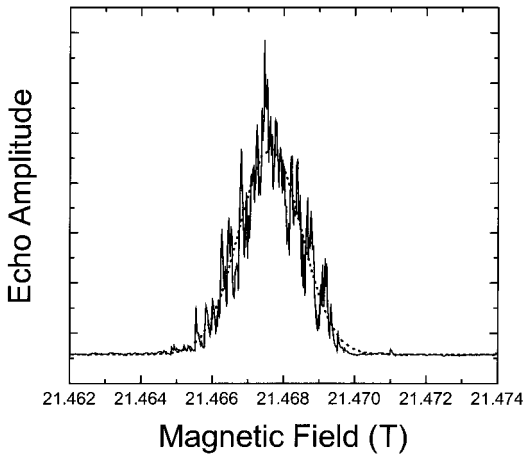

FIG. 13. Echo detected EPR spectrum of BDPA in polystyrene matrix, at a frequency of 604 GHz and a temperature of 8 K. The dotted line is a Gaussian fit. The jitter in the echo amplitude is due to the jitter of the external magnetic field.

$$\frac{1}{T_M} = \frac{1}{T_2} + \frac{1}{2T_1}. \qquad [20]$$

The procedure is to perform several two-pulse echo experiments for different interpulse times τ. The measurements were done with two independent far infrared lasers being triggered by a multichannel delay generator. The typical result is plotted in Fig. 14 for measurements on BDPA (1:10) at 4.9 K in a magnetic field of 21.442 T. The first and second excitation pulses are attenuated by the microwave switch with an isolation of 30 dB, where the opening of the switch is accompanied by noise, giving rise to some artificial peaks. We see clearly the echo height decreasing for long delays τ. If we take the echo heights as a function of τ (inset of Fig. 14) we can fit a first-order exponential decay ($\propto \exp(-2\tau/T_M)$) in order to determine the spin memory time T_M. For BDPA we obtain a T_M of 830 ns corresponding to a homogeneous linewidth of $\Gamma = 1/\gamma T_M \approx 0.13$ G.

The saturation recovery experiment is a three-pulse technique offering the opportunity to determine the spin–lattice relaxation rate T_1. An intense resonant pulse excites the spin system and takes it out of thermal equilibrium. Especially in high magnetic fields, the change of the level population can be very large due to the high initial spin polarization. The relaxation back to equilibrium is accomplished by coupling between the spins and the lattice characterized by T_1. The recovery of the initial population can be probed by a simple two-pulse echo sequence. If the time delay τ between the saturation pulse and the echo sequence is small the amplitude of the echo is small. By extending the delay we can observe an increase of the echo signal toward the echo amplitude of the equilibrium case, without saturation pulse.

In Fig. 15 we illustrate a typical result obtained on TEMPO in polystyrene (1:30) in a magnetic field of 21.506 T and at a temperature of 8 K. Curve (1) shows a three-pulse sequence with a very short delay time τ between saturation pulse and the two-pulse echo sequence, with a small echo amplitude. In comparison, the normal two-pulse result is given by curve (2). We recorded the echo amplitude for different τs and observe the recovery of the echo, which is plotted in the inset of Fig. 15. To determine the spin–lattice relaxation time T_1 we fit the Boltzmann function

$$E(\tau) = \frac{A - E(\infty)}{1 + \exp(\tau/T_1)} + E(\infty) \qquad [21]$$

with the three parameters A, $E(\infty)$, and T_1. The obtained value for T_1 is 10.3 μs $\pm$ 1.2.

5. SENSITIVITY

An exact determination of the sensitivity of the spectrometer is difficult because several values are not exactly known. For example, the attenuation in the oversized waveguides depends very critically on the alignment of the waveguide axis on the optical axis of the experiment. Nevertheless, we try to give an order of magnitude estimation of the expected sensitivity and compare this value with the experimentally determined sensitivity.

The emitted echo power following a free precession after a $\pi/2$ pulse is given by (*12, 38*)

$$P_e = \frac{\mu_0}{2}\,\omega_0 M_t^2 \eta Q_l V_s, \qquad [22]$$

where M_t is the transverse magnetization, which is $2\pi\mu_B N/V_s$, N being the number of contributing spins and V_s being the sample volume. The filling factor, η, defined as

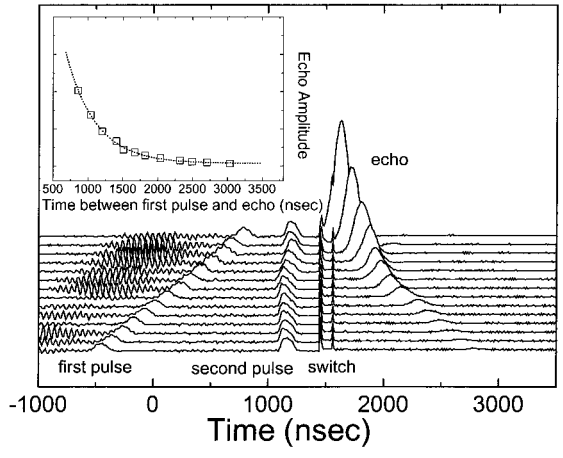

FIG. 14. Set of two-pulse echo measurements for different interpulse times τ on BDPA in polystyrene (1:10) at 4.9 K in 21.442 T. The inset shows the echo decay function being fit by $\exp(2\tau/T_M)$.

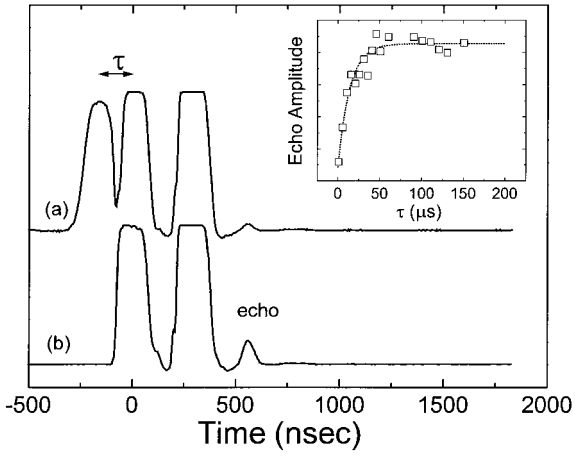

FIG. 15. (a) Saturation pulse sequence with attenuated echo. (b) Normal two-pulse echo. The inset shows the raising of the echo amplitude as a function of the delay between saturation pulse and echo sequence. The measurements are done on TEMPO (1:30) in a magnetic field of 21.506 and at a temperature of 8 K.

$$\eta = \frac{\int_{\text{sample}} B_1^2 dV}{\int_{\text{cavity}} B_1^2 dV}, \qquad [23]$$

depends on the geometry of the cavity. Q_l is the quality of the loaded cavity. Using appropriate numbers, $Q_l = 80$, $\eta = 0.01$, $V_s = 2.8 \times 10^{-9}$ m^3, we obtain a radiated echo power of

$$2.3 \times 10^{-30} N^2 \quad [\text{W}]. \qquad [24]$$

We want to point out that N is not the total number of spins but only the number of spins which are turned into the xy plane.

The generated echo power is transported in the oversized waveguides and only a fraction α reaches the detector. This value has to be compared with the detector threshold, the noise equivalent power. We have determined the noise-equivalent power in two ways: (1) in a hot–cold measurement the cw system noise temperature has been determined to be 60,000 K. When we multiply this value by k_B we obtain a noise equivalent power of 8×10^{-19} W/Hz. Assuming a bandwidth of 1 GHz we obtain a noise power of about 10^{-9} W. (2) A more direct way of determining the noise power of the system is to compare it with a reference source. For this measurement we determine the power of the pulsed FIR laser with a calibrated detector (Technoexan F 150). The FIR pulses are then sent to the heterodyne detector and are attenuated until the noise level of the detection system is reached. We determined a noise power of about 10^{-8} W.

If we set the echo power equal to the noise power (10^{-8} W), assuming a value of $\alpha = 1/50$, we estimate the number of detectable spins to be

$$N = 4 \times 10^{11}. \qquad [25]$$

This value can be compared with the experimentally determined value. For a sample with an absolute number of 10^{16} spins, we obtain a signal to noise value of 10,000 and an EPR linewidth of about 100 G. If we assume that only 1/30 of the spins are in resonance with the FIR pulses, we obtain for the detection limit $10^{16}/(30\sqrt{10{,}000}) = 3 \times 10^{12}$ spins. This value corresponds within one order of magnitude to the theoretically estimated value.

The value for the sensitivity is not very impressive, but the spectrometer has been set up as a test spectrometer to see how electron-spin-echo spectroscopy can be performed using optical techniques. The above considerations show at once the "weak points" in the setup, which can be improved in order to increase the sensitivity: (1) the quality factor of the cavity, (2) the losses in the oversized waveguides, and (3) the sensitivity of the detection system. We think that it is possible to increase the sensitivity by several orders of magnitude.

6. CONCLUSION

We have constructed an electron-spin-echo spectrometer with an operating frequency of 604 GHz, which is more than a factor of 4 higher than ESE spectrometers reported before. In order to achieve this we have chosen a different approach than in existing spectrometers, because these high frequencies cannot easily be handled with conventional microwave/millimeter-wave techniques. As high-frequency source we have chosen pulsed FIR lasers and we have employed quasi-optical techniques for the beam transport, the cavity, and the detection, described in the experimental part of this work. Two pulsed and one cw FIR laser system are synchronized in the experimental setup.

Although the spectrometer is not as versatile as the well-established spectrometers that work at lower frequencies, it demonstrates that pulsed EPR at very high magnetic fields above 20 T is possible. To the best of our knowledge we have performed the first electron spin echo experiments using optical and not conventional microwave techniques. We have shown that we can produce two- and three-pulse sequences to measure the spin–spin and the spin–lattice relaxation times. Due to its construction principle (quasi-optical techniques), the spectrometer is not limited to only 604 GHz. With an improved cavity and beam transport, a variety of different FIR lines could be used, which would be particularly interesting for studying the frequency dependence of relaxation times.

A practical difficulty has been that the setup in the resistive 25-T magnet of the Grenoble High Magnetic Field Laboratory was not permanent, but had to be moved out after each measurement period. The installation and alignment of the lasers is time-consuming and makes it particularly difficult to operate the FIR lasers in the most stable conditions. This is, of course, in principle no restriction, because very stable and mobile FIR laser systems exist. However, in these setups the advantage of mobility is at the cost of very careful preparation periods,

which require a lot of manpower. We think that the sensitivity in a permanent setup could be increased by several orders of magnitude, improving the light guiding, the cavity, and the detection system.

Our constructed spectrometer is interesting for the study of many samples due to its overwhelming g resolution. For example, in TEMPO the hyperfine interaction determines the linewidth at conventional 9.5 GHz, whereas at 604 GHz the linewidth due to the anisotropic g tensor becomes dominant. In this way it is possible to perform orientational studies in powder samples by selecting a certain magnetic field. The relaxation times for a chosen molecule or crystallite orientation provide information about the structural and dynamical properties of the environment surrounding the probe. This is particularly interesting for biological samples where single crystals are not available and the hyperfine interactions are larger than the g anisotropy at low frequencies.

The spectrometer is interesting not only for applied studies, but also for fundamental investigations of spin dynamics at these high Zeeman splittings (2.5 meV at 604 GHz for $g = 2$). The finding of very long spin-memory times for samples with a relatively high spin concentration has been assigned to an almost complete spin polarization at these high frequencies/fields (*17*). By relatively concentrated samples, we mean that the individual spins cannot be regarded as isolated but are coupled due to dipolar or exchange interaction. The fact that the spin-memory times become longer with increasing frequencies makes the spectrometer particularly interesting for the study of substances which have too short relaxation times at conventional frequencies (coupled and correlated spin systems).

REFERENCES

1. E. L. Hahn, *Phys. Rev.* **80,** 580 (1950).
2. E. L. Hahn and D. E. Maxwell, *Phys. Rev.* **88,** 1070 (1952).
3. R. V. Blume, *Phys. Rev.* **109,** 1867 (1958).
4. W. B. Mims, K. Nassau, and J. D. McGee, *Phys. Rev.* **123,** 2059 (1961).
5. J. P. Gordon and K. D. Bowers, *Phys. Rev. Lett.* **1,** 368 (1958).
6. D. E. Kaplan, M. E. Browne, and J. A. Cowen, *Rev. Sci. Instrum.* **32,** 1182 (1961).
7. G. Feher, *Phys. Rev.* **103,** 834 (1956).
8. R. R. Ernst, G. Bodenhausen, and A. Wokaun, "Principles of Nuclear Magnetic Resonance in One and Two Dimensions," Clarendon, Oxford (1986).
9. T. S. Lin, *Chem. Rev.* **84,** 1 (1984).
10. J. R. Norris, M. C. Thurnauer, and M. K. Bowman, *Adv. Biol. Med. Phys.* **17,** 365 (1980).
11. J. Schmidt and D. J. Singel, *Annu. Rev. Phys. Chem.* **38,** 141 (1987).
12. R. Weber, J. A. J. M. Disselhorst, L. J. Prevo, J. Schmidt, and W. T. Wenckebach, *J. Magn. Reson.* **81,** 129 (1989).
13. T. F. Prisner, S. Un, and R. G. Griffin, *Israel J. Chem.* **32,** 357 (1992).
14. Ya. S. Lebedev, *in* "Modern Pulsed and Continuous-Wave Electron Spin Resonance (L. Kevan and M. K. Bowman, Eds.), Wiley, New York (1990).
15. W. B. Lynch, K. A. Earle, and J. H. Freed, *Rev. Sci. Instrum.* **59,** 1345 (1988).
16. F. Müller, M. A. Hopkins, N. Coron, M. Grynberg, L. C. Brunel, and G. Martinez, *Rev. Sci. Instrum.* **60, 12,** 3681 (1989).
17. C. Kutter, H. P. Moll, J. van Tol, H. Zuckermann, J. C. Maan, and P. Wyder, *Phys. Rev. Lett.* **74,** 2925 (1995).
18. A. Witowski, C. Kutter, and P. Wyder, *Phys. Rev. Lett.* **78,** 3951 (1997).
19. L. C. Brunel, T. M. Brill, I. Zaliznyak, J. P. Boucher, and J. P. Renard, *Phys. Rev. Lett.* **69,** 1699 (1992).
20. H. P. Moll, J. van Tol, M. S. Tagirov, D. A. Tayurskii, and P. Wyder, *Phys. Rev. Lett.* **77,** 3459 (1996).
21. C. P. Poole, "Electron Spin Resonance, a Comprehensive Treatise on Experimental Techniques," Interscience, New York (1967).
22. R. S. Alger, "Electron Paramagnetic Resonance, Techniques and Applications," Interscience, New York (1968).
23. S. A. Self, *Appl. Opt.* **22**(5), 685 (1983).
24. H. P. Röser, M. Yamanaka, R. Wattenbach, and G. V. Schultz, *Int. J. Infrared Millimeter Waves* **3,** 839 (1982).
25. H. J. Schneider-Muntau, *IEEE Trans. Magn.* **17,** 1775 (1981).
26. W. Schatz, M. A. Heusinger, R. S. Nebosis, K. F. Renk, and P. T. Lang, *Infrared Phys.* **34,** 339 (1993).
27. J. Burghoorn, "Time-Resolved Far-Infrared Spectroscopy," Ph.D. Thesis, Technische Universiteit Delft (1992).
28. E. V. Loewenstein and D. C. Newell, *J. Opt. Soc. Am.* **59,** 407 (1969).
29. N. Marcuvitz, "Waveguide Handbook," MIT Radiation Laboratory Series, McGraw–Hill, New York (1951).
30. E. A. J. Marcatili and R. A. Schmeltzer, *Bell Sys. Tech. J.,* 1783 (July 1964).
31. A. E. Siegmann, "Laser," University Science, Mill Valley, CA (1986).
32. L. Genzel, K. L. Barth, and F. Keilmann, *J. Infrared Millimeter Waves* **11,** 1133 (1990).
33. G. W. Chantry, *J. Phys. E. Sci. Instrum.* **15,** 3 (1982).
34. H. Salzmann, T. Vogel, and G. Dodel, *Opt. Commun.* **47,** 340 (1983).
35. R. Titz, B. Auel, W. Esch, H. P. Röser, and G. Schwaab, *Infrared Phys.* **30,** 435 (1990).
36. O. Hachenberg and B. Vowinkel, "Technische Grundlagen der Radioastronomie," Bibliographisches Institut, Mannheim (1982).
37. M. S. Tobin, *Proc. IEEE* **73,** 61 (1985).
38. J. Allgeier, J. A. J. M. Disselhorst, R. T. Weber, W. T. Wenckebach, and J. Schmidt, *in* "Modern Pulsed and Continuous-Wave Electron Spin Resonance," (L. Kevan and M. K. Bowman, Eds.), Wiley, New York (1990).